OPTICAL PROCESSES IN MICROCAVITIES

A new generation of optical microresonators is making possible the exploration of quantum electrodynamic phenomena in condensed matter systems and providing microlasers with a wide range of potential applications.

Yoshihisa Yamamoto
and Richart E. Slusher

Studies of optical microresonators with dimensions between 0.1 and 10 microns are now under way in a wide variety of condensed matter systems. Ideally, one can isolate a single mode of the optical field in a cube a half-wavelength on a side with perfectly reflecting walls. Liquid droplets, polymer spheres and semiconductor Fabry–Perot microcavities with dielectric mirrors are examples of microresonators with which one can approach this ideal limit and nearly isolate a few modes of the electromagnetic field from the continuum of surrounding free-space modes.

The interaction of optically active material in the form of dyes or semiconductor quantum wells with these isolated modes offers interesting physical systems for basic studies and a rich variety of possible applications. Interactions between atoms and low-loss optical and microwave cavities have led to beautiful demonstrations of cavity quantum electrodynamic effects in recent years, including coupled atom–cavity modes, quantum revivals, single-atom masers and enhanced or inhibited spontaneous emission.[1] (See the article by Serge Haroche and Daniel Kleppner in PHYSICS TODAY, January 1989, page 24.) Microfabrication techniques are now making some of these QED phenomena accessible for study in condensed matter systems.

Semiconductor microlasers are a good example of condensed matter microcavities. A rich variety of cavity resonator geometries, including "baseball bats," hemispheres and "thumbtacks," have been fabricated using modern photolithographic and etching processes. (See figure 1.)

Optical gain in the active region of these resonators can dominate optical loss when optical or electrical carrier injection creates a population inversion in the semiconductor's valence and conduction bands. At low carrier injection rates a particular mode of a semiconductor microresonator will be occupied on the average by less than one photon as a result of spontaneous emission produced by carriers making transitions from conduction to valence states. One can view the vacuum fluctuation fields in the cavity mode as the generator of this emission

Yoshihisa Yamamoto is a professor of applied physics and electrical engineering at Stanford University and a research group leader at the NTT Basic Research Laboratory, in Tokyo, Japan. **Richart Slusher** is head of the optical physics research department at AT&T Bell Laboratories in Murray Hill, New Jersey.

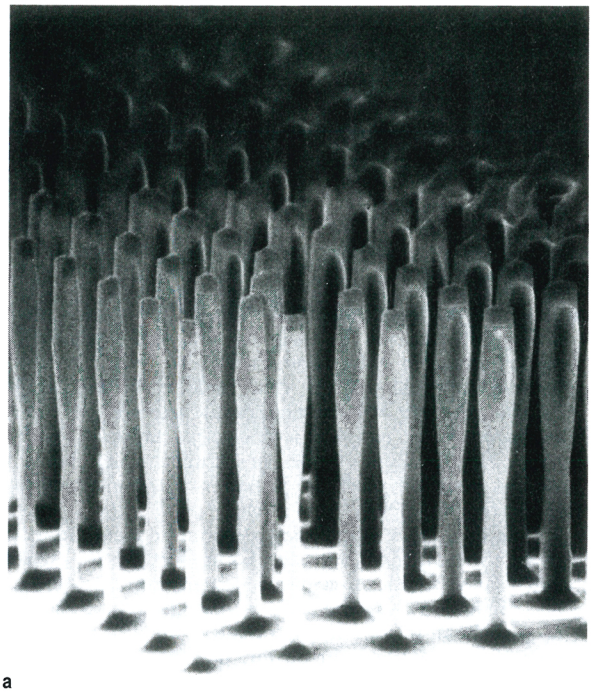

a

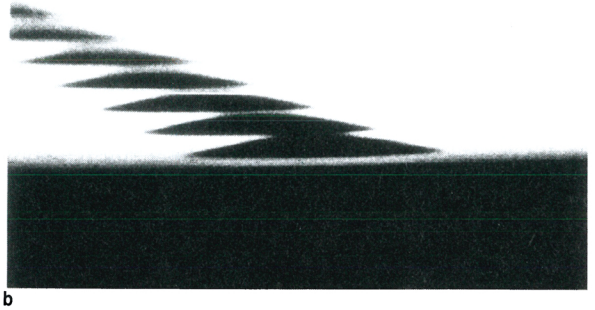

b

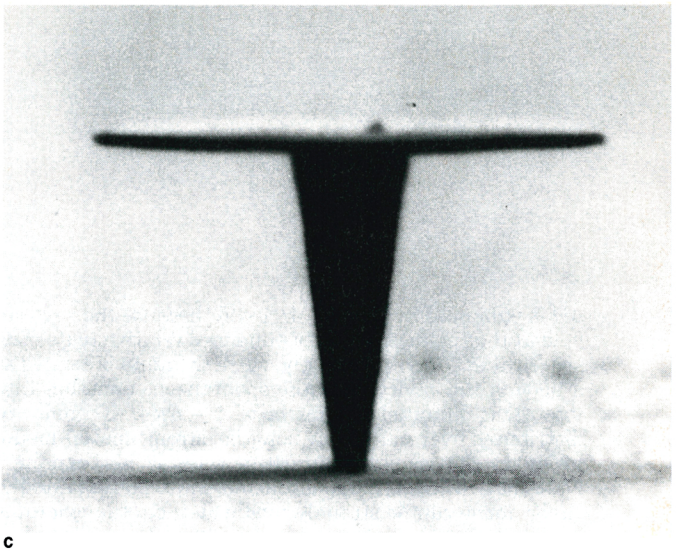

c

Microlasers as seen with a scanning electron microscope. **a:** Semiconductor microlasers in a Fabry–Perot configuration using the GaAs–AlGaAs system. (Courtesy of Jack Jewell, Photonics Research Inc, and Axel Scherer, Bellcore.) **b:** Hemispherical GaAs structures. **c:** Microdisk structure using the InGaAs–InGaAsP system. Lasing is achieved in these structures by optical pumping. The baseball-bat shaped microcavities in **a** are as small as 0.4 microns in diameter; the hemispheres in **b** are 7 microns in diameter; the microdisk in **c** is only 0.15 microns thick. These small dimensions cause there to be only a few dominant modes in the spectral gain region. **Figure 1**

process. As the carrier pump rate is increased, a lasing threshold is reached when there is approximately one photon on average in the lasing mode. At this threshold pump rate, stimulated emission by the optical field in the microcavity begins to dominate spontaneous emission. As the pump rate is increased above threshold, the spectral linewidth of the radiation emerging from the microcavity is expected to narrow relative to the spontaneous emission linewidth, and the radiation pattern is dominated by the spatial characteristics of the lasing mode.

Cavity quantum electrodynamics

One can use the quantum electrodynamic theory of spontaneous emission to calculate the decay rate and frequency shift resulting from vacuum field fluctuations acting on an atom in free space. For instance, a QED frequency shift for the 2s state of a hydrogen atom is calculated to be 1040 MHz by the nonrelativistic QED theory, a value that is very close to the measurement of 1057 MHz obtained by Willis E. Lamb Jr and R. C. Retherford. A common misunderstanding is that the spontaneous emission rate and the frequency shift are inherent properties of an atom. In fact the spontaneous emission rate is not an immutable property of an atom but a consequence of atom–vacuum field coupling, and it would disappear if there were no vacuum field fluctuations. The vacuum field fluctuates and polarizes the atom, and in return the induced atomic dipole fluctuates and polarizes the vacuum field. With this physical interpretation of spontaneous emission in mind, it is not surprising that one can tailor the decay rate and frequency shift by using a cavity wall to modify the vacuum field fluctuations.

Because spontaneous emission is a major source of energy loss, speed limitation and noise in lasers, the capability to control spontaneous emission is expected to improve laser performance. New phenomena are expected if the radiation pattern is highly directed toward a lasing mode and the fraction of spontaneous emission coupled into the lasing mode is made close to 1. The fraction of the total spontaneous emission that is coupled into the single lasing mode at low excitation rates is defined to be the spontaneous emission coefficient β. An example of the new phenomena expected as β approaches 1 is the "thresholdless laser,"[2,3] in which the light output increases nearly linearly with pump power instead of exhibiting a sharp turn-on at a pump threshold.

Consider a single atom centered in an optical cavity between two confocal mirrors, each with reflectivity R. This cavity radiates into a mode that subtends a solid angle $\Delta\Omega$. If the atom is located at an antinode of the vacuum field in the cavity, the spontaneous emission rate into

$\Delta\Omega$ is enhanced by a factor $4/(1-R)$ because the vacuum field at that point is strongly enhanced relative to its free-space value. Correspondingly, when the atom is located at a node of the cavity field, the spontaneous emission rate into $\Delta\Omega$ is inhibited by a factor of $(1-R)/4$. If atoms are distributed over many wavelengths, strong spatial modulation of the spontaneous decay rates is not expected. Note that although the spontaneous emission rate into the cavity mode can be strongly modified, the total spontaneous emission rate integrated over all angles may change only a modest amount if $\Delta\Omega \ll 4\pi$.

The most important effect of modified spontaneous emission for possible applications is the altered radiation pattern and the enhanced spontaneous emission coefficient β. The strong reflectivity dependence of the spontaneous emission rate into a cavity mode clearly indicates that β can be increased when an atom is located at the antinode of the mode field. As the reflectivity approaches unity the β value approaches the ideal limit of 1. Such high β values can be used to enhance the efficiency of light-emitting diodes and lower the thresholds of lasers.

Microcavity laser physics

The spontaneous emission coefficient β for the relatively large-volume solid-state and gas lasers in common use today can be approximated by[4]

$$\beta = \frac{\lambda^4}{4\pi^2 V \Delta\lambda n^3} \tag{1}$$

Here $\Delta\lambda$ is the emission linewidth, n the refractive index and V the mode volume. This expression accounts for the number of modes in the system, which is roughly equal to the number of cubic wavelengths in the system, and the number of modes within the emission linewidth, which is proportional to $\Delta\lambda/\lambda$. For example, even a semiconductor laser the size of a grain of salt has a β value of only 10^{-5}. One can reduce both V and $\Delta\lambda$ to obtain a larger β value. In principle one can increase the β value to close to 1. For this purpose, one does not necessarily require a true single-mode cavity. One needs only to enhance the spontaneous emission rate into a single mode relative to the many existing modes over the spectral emission bandwidth, which is typically less than a few percent of the transition frequency.

One of the most important consequences of the increased spontaneous emission coefficient is the reduction of the threshold pump rate of a laser. In a simple atomic model, where the spontaneous emission rate and the emission spectral width are constant as a function of excitation level, the threshold pump rate as a function of β is given by[5]

$$P_{th} = \frac{\gamma_{photon}}{2\beta}\left[1+\beta+\xi(1-\beta)\right] \tag{2}$$

Here γ_{photon} is the rate of photon emission from the cavity. The quantity $\xi = N\beta V\Gamma/2\gamma_{photon}$ is the average photon number in the lasing mode when half of the atoms are in the excited state; N is the atomic density and Γ is the spontaneous emission rate. The excitation level where the excited-atom density N_{ex} is $N/2V$ is called the transparency carrier density in semiconductors, because there is no absorption and no net gain at this point. The gain G at excitation levels higher than the transparency point is assumed here to be a linear function of the excited-atom density N_{ex}: $G = \beta V\Gamma(N_{ex} - N/2)$.

The threshold pump rate in equation 2 includes the two distinct regions that are being studied in present semiconductor microresonator experiments, $\xi \ll 1$ and $\xi \gg 1$. When $\xi \ll 1$ and $\beta \ll 1$, P_{th} is equal to $\gamma_{photon}/2\beta$ and the threshold pump rate decreases linearly with $1/\beta$. Figure 2 shows the light output power as a function of pump rate for a set of β values in this regime. The lasing threshold, characterized by the jump in the efficiency of converting pump power to light output power, decreases with increasing β. When $\xi \gg 1$ and $\beta \ll 1$, P_{th} is independent of β and is fixed at the pump rate required to obtain transparency. One must keep the total number of atoms NV and the spontaneous decay rate Γ small to satisfy the condition $\xi \ll 1$ and obtain a decrease in the threshold pump rate with an increase in β. Of course, we are assuming that the active material can be pumped to emit a sufficient number of photons to achieve threshold at these low gain volumes. In practice the linear gain dependence assumed in this analysis cannot be achieved if the gain volume is too small. Another consequence of experimental reality is that β can vary with excitation level if the spectral emission width is not a constant.

In figure 2 we see that when the spontaneous emission coefficient β is 1 there is no jump in the quantum efficiency of the conversion of pump photons to light output. This is the "thresholdless" laser, or "zero-threshold" laser.[2] However, there is a well-defined threshold, $P_{th} = \gamma_{photon}$, even in this case, according to equation 2. At pump rates below threshold, the average photon number in the cavity is less than 1, so that the dominant emission process is incoherent spontaneous emission. At pump rates above threshold, the average photon number becomes greater than 1, resulting in a dominance of coherent stimulated emission. With the onset of stimulated emission, the population inversion is "pinned" at its threshold value, because each newly generated electron–hole pair very rapidly recombines in a stimulated process. The dominance of stimulated emission above threshold is also expected to result in an increased coherence of the light output and a narrowing of the output spectrum even in the $\beta = 1$ limit, as shown in figure 3a.

Fluctuations of the light intensity emitted by a microlaser exhibit a resonance increase at threshold, as shown in figure 3b. These light fluctuations, similar to the fluctuations found in a second-order phase transition, are a measure of threshold behavior that also persists in the limit of $\beta = 1$. Note that as β approaches 1, these fluctuations decrease and their relative width in pump

Three Kinds of Microcavities

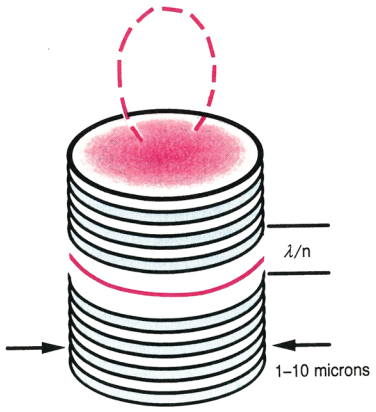

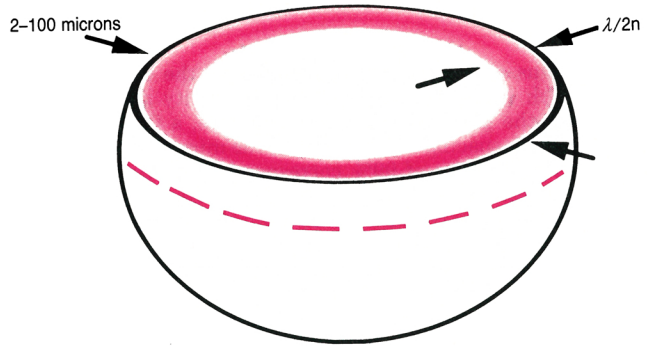

Three approaches to fabricating condensed matter optical microcavities are shown here schematically.

Micro-Fabry–Perot cavities (upper left) are fabricated using molecular-beam epitaxy to grow dielectric layered mirrors, shown as the alternately colored layers at the top and bottom of the cylinder. The active quantum well layer, typically GaAs, is shown as the red layer. The cylindrical boundary is formed by an etching procedure that results in structures that are typically 1–10 microns in diameter. The dominant mode pattern emitted from this cavity is shown as the dashed red line.

"Whispering gallery" modes, shown as the red shaded region in the figure at upper right, emit symmetrically outward from spherical or disk-shaped (indicated by the dashed line) structures. Liquid microdroplets as well as semiconductor disks and cylinders have been used in this configuration to form microlasers.

A defect mode in a periodic dielectric structure can in principle serve as a microresonator that completely isolates the microcavity mode from the free-space-continuum modes. The figure at lower right shows, for example, an acceptor defect (red shaded region) in a photonic bandgap structure. Structures of this sort have not yet been demonstrated as microlasers.

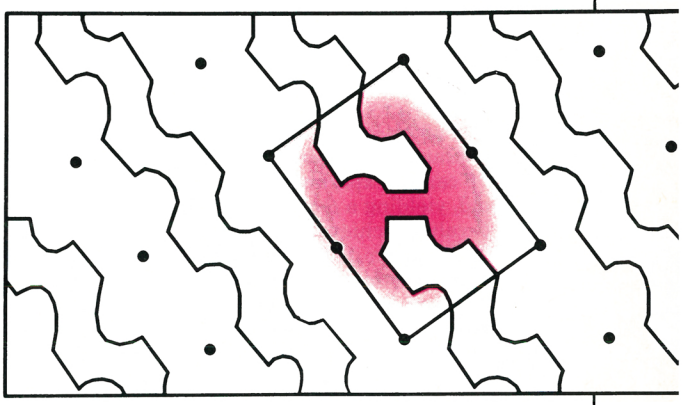

power increases, thus providing another indicator of the unique characteristics in the high-β microlaser limit.

We conclude from an examination of carrier density pinning, linewidth narrowing and light-level fluctuations—present even when there is only approximately one photon in the cavity—that there is a well-defined threshold even for $\beta = 1$. This threshold discriminates between regions that can be described as a linear amplifier and a nonlinear laser oscillator.

Fabry–Perot microcavities

The simplest approach to fabricating an optical microcavity is to shrink the spacing between the mirrors of a Fabry–Perot resonator to λ/n while reducing the lateral dimensions to the same range, as shown in figure at upper left in the box above. This structure provides a single dominant longitudinal field mode that radiates into a narrow range of angles around the cavity axis. The first optical microcavity experiments used dye molecules between high-reflectivity dielectric mirrors in the Fabry–Perot configuration.[3]

Semiconductor microcavities provide high-Q Fabry–Perot cavities for both basic studies and potential applications. The Q of a cavity is the number of radian cycles required for the optical field energy in the cavity to decay by a factor of $1/e$. Molecular-beam epitaxy or organometallic chemical vapor deposition techniques are used to deposit high-reflectivity mirrors consisting of alternating quarter-wavelength layers of lattice-matched semiconductors. For example, 15 to 20 pairs of quarter-wave layers of $Al_{0.2}Ga_{0.8}As$ and AlAs result in a reflectivity greater than 99% and Q values greater than 500. The optically active layer in such a microcavity is typically a GaAs quantum well located at the midplane of the cavity, where the field strength is a maximum. Figure 1a shows an example of the very-small-diameter microcavities that can be achieved by photolithographic patterning and etching of these layered materials; here the cylindrical cavities look like baseball bats.

Planar Fabry–Perot microcavities have been studied theoretically and experimentally in some detail.[6] The two important parameters for laser performance, γ_{photon} and β, depend on the cavity geometry and the spectral emission width of the quantum well gain material. Even if the dimensions of the cavity in the plane between the mirrors are much larger than an optical wavelength, the planar cavity structure will give rise to discrete spatial modes with a finite mode radius r_m. The mirror spacing and reflectivities determine the radiating solid angle of the mode. This solid angle is inversely proportional to the

coherence radius and directly proportional to the cold-cavity linewidth $\Delta\lambda_m$—the linewidth of the cavity resonance without the gain material. For example, a GaAs microcavity with a spacing of λ/n between the mirrors and with mirror reflectivities of 99% corresponds to a mode radius $r_m \simeq 7$ microns, a cavity resonance linewidth $\Delta\lambda_m \simeq 0.43$ nm and a far-field angular radiation angle of 5.7°.

The maximum β achievable with a large-area planar GaAs Fabry–Perot microcavity is estimated to be 0.05, assuming dipole moments oriented in the plane of the cavity and negligible spectral broadening. However, the GaAs quantum well emission linewidth is 30 nm at room temperature and 2.5 nm at 4 K, much broader than the cold-cavity linewidth of 0.43 nm. As soon as the emission linewidth exceeds the cold-cavity bandwidth, β starts to decrease with the ratio of the two widths; β is thus estimated to be $0.05(0.43/2.5) \simeq 0.01$ at 4 K. The quantum efficiency for conversion of pump photons to output light is close to unity above the threshold, while it is equal to β below it, assuming negligible absorption in the cavity. Therefore β can be experimentally deduced from the step at threshold, yielding a β of 10^{-2}, as shown in figure 4.

The β values achievable with the large-area planar microcavities are limited by the leakage of spontaneous emission into directions centered around the plane of the cavity.[4,6,7] A post-like structure, fabricated by wet or dry etching, can suppress this leakage of spontaneous emission and increase the β values up to 0.5 if the post diameter is on the order of the wavelength in the material and if the quantum well emission linewidth is much narrower than the cold-cavity linewidth.[4] (Figure 1a and the figure at upper left in the box on page 69 show post structures.) The factor-of-2 degradation in β stems from the fact that the two degenerate orthogonal polarization modes capture an equal amount of spontaneous emission below threshold, but only one of them oscillates above threshold. Such a high β has not yet been observed experimentally, in part because the emission linewidths are often broader than the cold-cavity linewidths.

An alternative way to increase β is to use a hemispherical structure with an integrated curved mirror.[8] Figure 1b shows a series of GaAs hemispherical cavities. To fabricate each of these curved mirrors, researchers formed a photoresist disk on a planar GaAs–AlGaAs optical cavity. They then melted this photoresist by heat treatment, forming it into a hemispherical disk. Finally they transferred the curved geometry of the photoresist disk to the semiconductor by dry etching using an ion beam. They controlled the curvature and diameter of the structures by varying the diameter and the thickness of the resist disk; the resulting curvatures ranged from 5 to 20 microns. The hemispherical microcavity has a measured β value of 0.05, which compares with the theoretical prediction of 0.1.

A variety of condensed matter Fabry–Perot microcavities have exhibited modifications of the spontaneous emission patterns and rates. Modified radiation patterns have been observed for the exciton emission from GaAs microcavities.[9] Dye-molecule experiments have demonstrated both enhanced and inhibited spontaneous emission rates.[10] One easily controls inhibition or enhancement in these experiments by adjusting the Fabry–Perot cavity spacing to set the position of the field node in the active dye layer. Narrowing of the emission angle and enhancement of the intensity of the emitted radiation have been observed[11] from erbium-doped glass in a Fabry–Perot cavity with mirrors formed from four alternate quarter-wave layers of silicon and SiO_2: The intensity of 1.54-micron radiation from the Er-doped glass along the cavity axis was enhanced by between one and two orders of magnitude, and the spectral width was narrowed by a factor of 10.

Microcathedrals

"Whispering gallery" modes are a second successful route to achieving high-Q microcavities. Total internal reflection along a curved boundary between two materials with

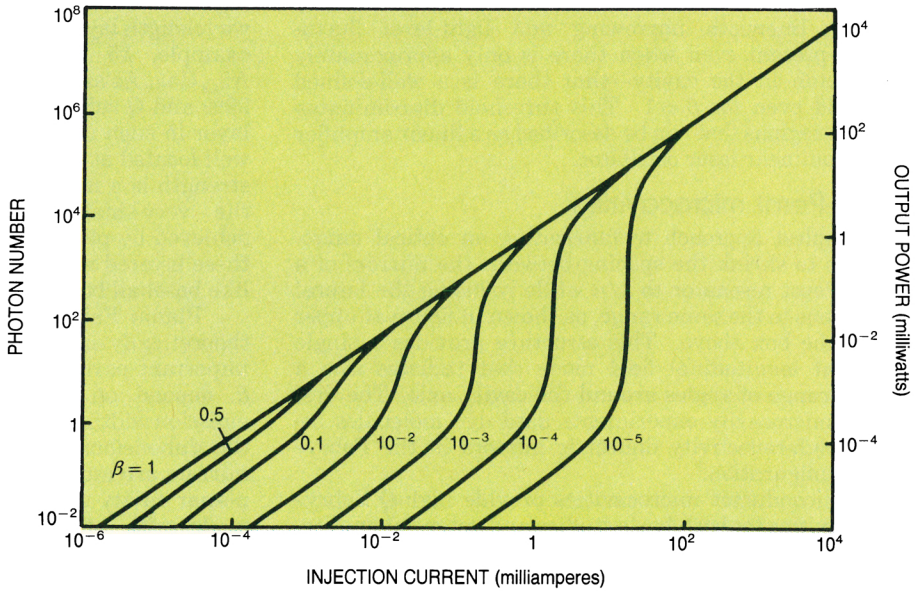

Photon flux and power. The curves show the average flux in the mode (left axis) and the corresponding output power (right axis) for microcavity lasers with various spontaneous emission coefficients β. Parameters used for the theoretical model that generated these curves are $\gamma_{photon} = 10^{12}$/sec, $\Gamma = 10^9$/sec, $N/V = 10^{18}$/cm^3, $V = 10^{-15}$ cm^3 and $\lambda = 1$ micron. **Figure 2**

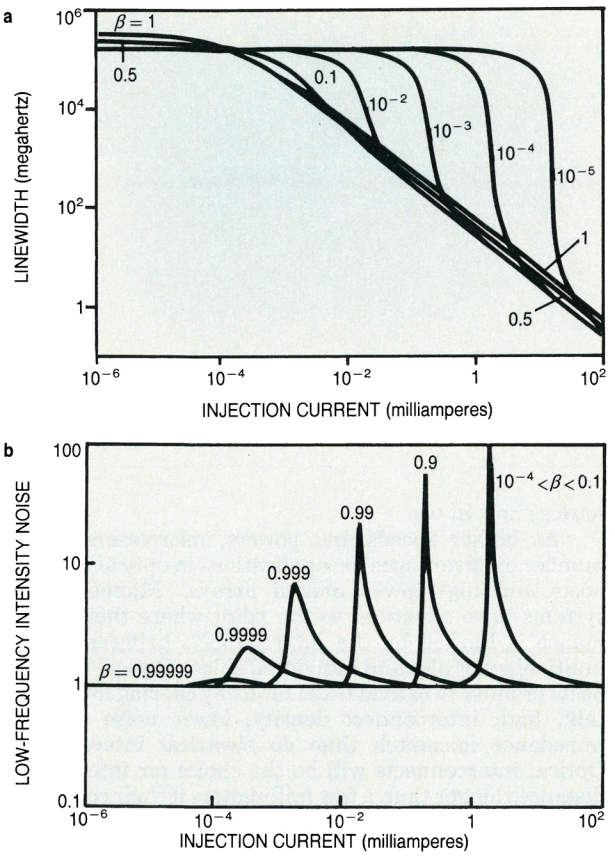

Linewidth and noise. The laser linewidth (**a**) and intensity-noise spectral density (**b**) in the light output from a microlaser as a function of the pump current are plotted here for a series of β values. The noise shown here is normalized with respect to the mean number of photons in the cavity. The parameters used in the theoretical model that generated these curves are the same as in figure 2. **Figure 3**

different optical indices results in high-Q modes propagating within a half-wavelength of the boundary, as shown in the figure at upper right in the box on page 69. Lord Rayleigh conceived these modes over a century ago as an explanation of the efficient propagation of sound—even of whispers—along the walls of St. Paul's Cathedral in London. In fact, the ratio of the sound wavelength to the cathedral diameter is very similar to the ratio of the light wavelength to the diameter of optical microcavities being studied today.

Whispering-gallery modes in condensed matter microstructures were pioneered using nearly spherical liquid droplets.[12] Cavities with Q values as high as 10^8 can be obtained because of the nearly perfect smoothness of the droplet boundaries, which in many cases is limited only by thermal fluctuations at the surface. Spectacular enhancements of the spontaneous decay rates of dye molecules—by a factor of 120—have been demonstrated in these microcavities.[13] Polymer spheres have now been fabricated with the optical smoothness required for high-Q whispering-gallery mode microcavities:[14] Optically pumping a dye-doped polystyrene sphere results in a red microlaser.

Researchers have demonstrated semiconductor whispering-gallery mode microresonators as microlasers in the disk and cylindrical geometries.[15] Figure 1c shows an InGaAs–InGaAsP microdisk resonator. The thickness of the disk is only 100 nm, less than a half-wavelength in the semiconductor, thus allowing only one transverse optical mode to propagate in the plane of the disk. This microcavity geometry allows an excellent overlap of the optical gain region with the mode volume. Large overlap factors are important for achieving low microlaser thresholds. This geometry avoids the complexity of multilayer mirrors and allows the fabrication of high-Q microcavities in systems like InGaAs–InGaAsP, where the index contrast for layered mirrors is not high enough to permit fabrication of high-reflectivity distributed Bragg reflectors. For a 1-micron-radius disk and an optical wavelength of 1.5 microns, there are approximately eight optical nodes arranged around the disk edge in a whispering-gallery mode. The spectral spacing of modes with differing numbers of nodes is large enough that only one mode dominates the InGaAs quantum well emission spectrum centered near 1.5-micron wavelengths. The measured[16] Q values for these 1-micron-radius microdisks range from 200 to 1000, and the β values are near 0.1, compared with the theoretically predicted value of 0.3.

Low-threshold microlasers

Optical microresonators promise ultralow-threshold laser behavior primarily because the threshold should scale down with the gain volume and with the increased coupling of spontaneous emission into the cavity mode—that is, with increased values of β. As the gain volume approaches a fraction of a cubic wavelength in the material and as β approaches 1, threshold powers below 1 microwatt are expected for sufficiently high Q values. This is a factor of nearly a thousand less than the thresholds near 1 milliwatt that are typical for semiconductor lasers in common use today with volumes of several hundred cubic wavelengths and β values that range from 10^{-4} to 10^{-5}.

Estimated thresholds have been demonstrated in the 5–10-μW range for Fabry–Perot semiconductor microlasers with one quantum well[6] and in the 10–20-μW range for whispering-gallery mode microlasers with six quantum wells.[16] These experiments used optical pumping and temperatures below that of liquid nitrogen. The actual pump light levels incident on the structures in these experiments range from 700 μW to 1 mW for the Fabry–Perot microcavities[7] and from 30 to 100 μW for the whispering-gallery mode microcavities.[16] Only the fraction of this power actually absorbed in the active region is used to obtain the estimated thresholds. Nonlasing modes reduce the β values in these microlaser experiments to the 0.01–0.1 range, because the total volumes of the cavities are still considerably larger than the ideal limit.

Electrically pumped room temperature microlasers will be needed for many applications.[17] Under such restrictions, threshold currents as low as 700 μA have been demonstrated for wavelengths near 0.8 microns in vertical-cavity surface-emitting Fabry–Perot microlasers using GaAs quantum wells,[18] as have threshold currents of 900 μA for wavelengths near 1.5 microns in microdisk lasers using InGaAs quantum wells.[19] A number of problems plague low-threshold microlasers in this regime, including electrical losses in the mirrors of the VCSEL structures and cooling for all microlasers. The route to achieving very low thresholds at room temperature includes cavities of higher Q (which is especially important for the very small gains of microlasers), larger gain–mode overlap factors,

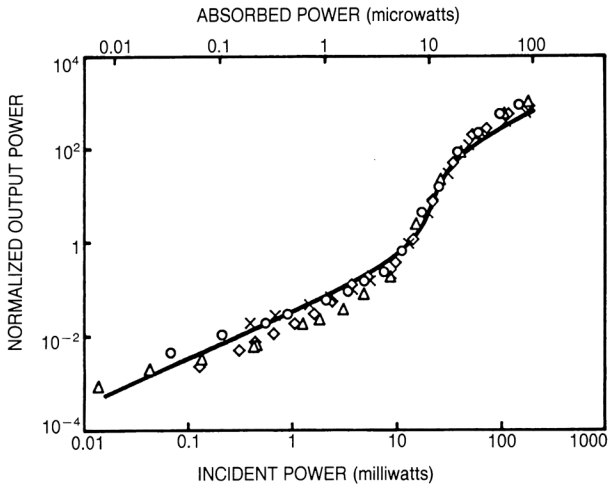

Power transfer. The normalized output power from a GaAs Fabry–Perot microcavity is plotted here as a function of incident pump power (bottom axis) and absorbed pump power (top axis). The solid line is the theoretical curve for $\beta = 0.01$. (The fraction of the total spontaneous emission that is coupled into the single lasing mode at low excitation rates is defined to be the spontaneous emission coefficient β.) (Data from ref. 6) **Figure 4**

decreased electrical series resistance and improved heat sinking.

Applications

Microcavity resonators have the potential to provide relatively low-cost, efficient and high-density optoelectronic light sources over a broad range of the spectrum, from the near-infrared to well into the visible. Low-cost, high-density light source arrays and photonic circuits are possible because of the small size and low power consumption of such resonators. One will be able to test entire wafers containing millions of microlasers with a multiprobe arrangement instead of having to cleave each individual semiconductor laser as at present. This improvement will lead to higher yields and lower cost per element. Another advantage of surface-emitting microcavity sources is the efficient optical coupling of their stable symmetric mode patterns into optical fibers or waveguides.

Efficient light-emitting diodes based on microresonators will be useful for low-speed, low-power applications. The efficiency of LED emission in a particular direction is enhanced because of the narrowed angular spontaneous emission pattern, the enhanced rates and the increased β value obtained with a microcavity. The time response of LEDs is typically limited by the radiative lifetime, which is on the order of nanoseconds for many semiconductors. Even this limitation can be overcome with the significantly enhanced spontaneous emission rates that may be obtained in microcavities. New, high-efficiency conducting organic polymers are another interesting possibility for the optically active material in a micro-LED.[20] Applications for micro-LEDs may include laser printers and read–write sources for optical memories and displays. Large arrays could serve as high-functionality replacements for the single or one-dimensional-array light sources now in use.

At higher speeds and powers, microlasers have a number of advantages for applications in optical interconnects and high-power phased arrays. Microelectronic systems have advanced to the point where their performance is limited by the interconnects between boards, multichip modules and individual chips. Optical interconnects promise to extend these limits by offering lower cross talk, high interconnect density, lower noise and less impedance mismatch than do electrical interconnects. Optical interconnects will be the choice for interconnect distances longer than a few millimeters if their cost can be reduced to a competitive range. Data rates in the range of 1 to 10 gigabits per second are of interest for the immediate future. At present generating logic-level voltages with a low-cost optical receiver requires coupling approximately 1 mW of power into an optical fiber. In the future, using microlasers with powers in the hundred-microwatt range and more sensitive receivers, much higher densities will be achievable.

Several laboratories are now fabricating two-dimensional arrays of electrically pumped surface-emitting microlasers. (Figure 5 shows one such array.) A group at Bellcore has demonstrated[21] individually addressable 32×32 arrays with thresholds between 6 and 8 mA. Daryoosh Vakshoori and his coworkers at AT&T Bell Laboratories have demonstrated[22] an 8×18 array of microlasers, each with a threshold current near 4 mA and a threshold voltage near 2.65 V. Each microlaser in the AT&T array operates at 450 megabits/sec, making the net potential throughput 65 gigabits/sec. The group has achieved operation for over 1000 hours without significant degradation in performance; however, complete reliability studies over a range of temperatures remain to be done. Each element of this array emits a symmetric Gaussian pattern with a low divergence angle that allows efficient coupling into optical fibers or other optics with low numerical apertures. One of the next steps in the evolution of this technology will be to incorporate "smart pixel" features that will allow logic operations with several transistors at each microlaser location.

Future

The present trends toward smaller-scale nanostructures and the continuous development of new and improved materials should result in steady progress toward more ideal optical microcavities. Examples of new materials include quantum wires and dots in semiconductor or organic systems. An interesting approach for achieving a truly isolated optical mode is the fabrication of three-

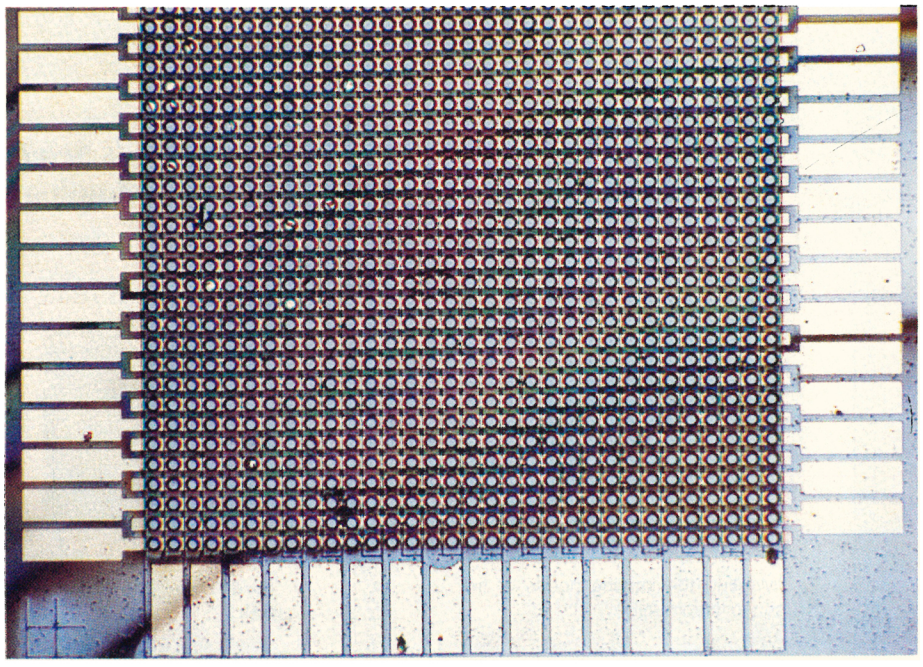

Laser array. This optical microscope image shows a 32×32 array of individually addressable, electrically pumped surface-emitting Fabry–Perot microcavities. Each laser is approximately 10 microns in diameter and has a threshold current of 3–4 milliamperes. (Photograph courtesy of Jewell.) **Figure 5**

dimensional photonic bandgap systems that exclude all optical modes over a limited optical spectrum.[23] An "acceptor" or "donor" optical mode with a frequency in this isolated spectral region can then be formed as a dielectric defect, as shown in the figure at lower right in the box on page 69. These defect modes can in principle form high-Q resonant modes with β values very close to 1. With advances in experimental systems, we may soon see a more substantial basis in experiment for the novel physics of QED, lasing without inversion, cavity-assisted excitonic superradiance and squeezed-light generation.[6]

The limit of isolated field modes in microresonators may also have a significant impact in applied areas. For example, if visible microlasers can be developed, their many potential applications include fast holographic memories, laser projection displays, plastic fiber optic communications and applications where HeNe lasers are used at present.

Many challenges remain in the application of optical microcavities, including improvement of the "wall plug" efficiency—the total conversion efficiency from electrical to laser-mode power—from present values near 10% to the 20–50% range. Aging and reliability are problems for many materials systems used in optical microcavities, including semiconductors and organic polymers. In spite of these problems several companies, including Photonics Research and AT&T, are searching for possible markets and systems applications for microcavity light sources.

References

1. S. E. Morin, Q. Wu, T. W. Mossberg, Optics & Photonics News, August 1992, p. 8.
2. F. DeMartini, G. R. Jacobovitz, Phys. Rev. Lett. **60**, 1711 (1988).
3. H. Yokoyama, K. Nishi, T. Anan, Y. Nambu, S. D. Brorson, E. P. Ippen, M. Suzuki, Opt. Quantum Electron. **24**, S245 (1992).
4. T. Baba, T. Hamano, F. Koyama, K. Iga, IEEE J. Quantum Electron. **27**, 1347 (1991).
5. G. Björk, Y. Yamamoto, IEEE J. Quantum Electron. **27**, 2386 (1991).
6. Y. Yamamoto, G. Björk, H. Heimann, R. Horowicz, in *Optics of Semiconductor Nanostructures*, F. Henneberger, S. Schmitt-Rink, E. O. Göbel, eds., VCH, Weinheim, Germany (1993), p. 275.
7. Y. Yamamoto, S. Machida, G. Björk, Phys. Rev. A **44**, 657 (1991).
8. F. M. Matinaga, A. Karlsson, S. Machida, Y. Yamamoto, T. Suzuki, Y. Kadota, M. Ikeda, Appl. Phys. Lett. **62**, 443 (1993).
9. Y. Yamamoto, S. Machida, K. Igeta, Y. Horikoshi, in *Coherence and Quantum Optics VI*, J. H. Eberly, L. Mandel, E. Wolf, eds., Plenum, New York (1989), p. 1249.
10. F. De Martini, M. Marrocco, P. Mataloni, L. Crescentini, R. Loudon, Phys. Rev. A **43**, 2480 (1991).
11. E. F. Schubert, A. M. Vredenberg, N. E. J. Hunt, Y. H. Wong, P. C. Becker, J. M. Poate, D. C. Jacobson, L. C. Feldman, G. J. Zydzik, Appl. Phys. Lett. **61**, 1381 (1992).
12. H. M. Tzeng, K. F. Wall, M. B. Long, R. K. Chang, Opt. Lett. **9**, 499 (1984).
13. A. J. Campillo, J. D. Eversole, H.-B. Lin, Phys. Rev. Lett. **67**, 437 (1991).
14. M. Kuwata-Gonokami, K. Takeda, H. Yasuda, K. Ema, Jpn. J. Appl. Phys. Lett. **31**, 99 (1992).
15. S. L. McCall, A. F. J. Levi, R. E. Slusher, S. J. Pearton, R. A. Logan, Appl. Phys. Lett. **60**, 289 (1992).
16. R. E. Slusher, A. F. J. Levi, U. Mohideen, S. L. McCall, S. J. Pearton, R. A. Logan, Appl. Phys. Lett. (1993), to be published.
17. Y. H. Lee, J. L. Jewell, A. Scherer, S. L. McCall, J. P. Harbison, L. T. Florez, Electron. Lett. **25**, 1377 (1989).
18. R. S. Geels, L. A. Coldren, Electron. Lett. **27**, 1359 (1991).
19. A. F. J. Levi, R. E. Slusher, S. L. McCall, T. Tanbun-Ek, D. L. Coblentz, S. J. Pearton, Electron. Lett. **28**, 1010 (1992).
20. J. H. Burroughs, D. D. C. Bradley, A. R. Brown, R. N. Marks, K. D. Mackay, R. H. Friend, P. L. Burn, A. B. Holmes, Nature **347**, 539 (1990).
21. M. Orenstein, A. C. Von Lehmen, C. Chang-Hasnain, N. G. Stoffel, J. P. Harbison, L. T. Florez, Electron. Lett. **27**, 437 (1990).
22. D. Vakshoori, J. D. Wynn, G. J. Zydzik, R. E. Leibenguth, submitted to Appl. Phys. Lett. (available from Slusher).
23. H. O. Everitt, Optics & Photonics News, November 1992, p. 20. P. L. Gourley, M. E. Warren, G. A. Vawter, T. M. Brennan, B. E. Hammons, Appl. Phys. Lett. **60**, 2714 (1992). ■